A comparison of the structure of the aerosol layers in the great red spot of Jupiter and its surroundings before and after the 1993 SEB disturbance

Olga Muñoz[1,2], **Fernando Moreno**[1], **Antonio Molina**[1,3], and **José L. Ortiz**[1]

[1] Instituto de Astrofísica de Andalucía, CSIC, P.O. Box 3004, E-18080 Granada, Spain
[2] ESA external fellowship at the Department of Physics and Astronomy, Free University, Amsterdam, The Netherlands
[3] Departamento de Física Aplicada, Universidad de Granada, Spain

Abstract. The structure of the aerosol layers in the Great Red Spot (GRS) of Jupiter is investigated from high-quality CCD ground-based observations. The observation of the feature was made at a variety of wavelengths at UV through the near-infrared and at different observational geometries as the large oval rotated from the central meridian to the limb, and at different times, specifically before and after the 1993 major South Equatorial Belt Disturbance (SEBD) on the planet. The particle size distribution as a function of height at tropospheric to lower stratospheric levels was retrieved at the different times observed, as well as the variation of the particle index of refraction as a function of wavelength. The total column abundance of particles above the 500 mbar level was found to be 2.3×10^8 cm^{-2}, with particle sizes ranging from 0.18 to 0.60 μm, depending on pressure level. A comparison with the ambient atmosphere that surrounds the GRS indicates that the difference in colour between the feature and its neighborhood could be due to a different particle size rather than to a different refractive index of the particles. The average size of the particles above 500 mbar was different just before the SEBD as compared with their average size after the disturbance. The largest differences in size were found near the 120 mbar level (50% smaller after the SEBD). The analysis of the observations made just after the disturbance on June 1993 and a year after the disturbance on July 1994 reveals that the particle size and their optical properties remained constant throughout this period.

Key words: radiative transfer – planets and satellites: individual: Jupiter

1. Introduction

The Great Red Spot (GRS) is the most prominent and long-lived feature on Jupiter. Despite the fact that it has been observed for more than 300 years (see Peek 1958 for an overview of these ground-based records), many unanswered questions on this oval region still remain. One of the most striking characteristics is its coloration. A different material and/or particle size distribution compared to its surroundings should overly this feature. The different reflective properties of the spot compared to its surroundings is best seen in images taken through blue and ultraviolet filters, where the GRS is darker than the ambient atmosphere, and through a methane band filter at 8900 Å wavelength, where the feature is much brighter than the adjacent regions. Aerosol particles play a crucial role by modifying the reflectivity on the different Jovian atmospheric regions, in particular the GRS and, in part, driving the motions by the heating rates at different Jovian atmospheric levels.

After the detection of phosphine (PH_3) in the Jovian atmosphere (Ridgway 1974), solid elemental phosphorus (P_4) produced by the photolytic decomposition of PH_3, was proposed to be the main candidate for the source of the red coloration of the GRS (Prinn & Lewis 1975). Based on laboratory measurements of UV photolysis of mixtures of phosphine in hydrogen and a Jovian GRS spectrum, (Noy et al. 1981) inferred a value of 0.05 μm for the radius of the particulates over the GRS, provided phosphorus is causing the red coloration of the feature. At present, we have not found any other published estimates of the GRS particle physical properties.

The purpose of this work is to study the Jovian aerosols on the GRS based on imaging at various wavelengths in the ultraviolet through 9500 Å, including observations in the 8900 Å methane absorption band region. We took advantage not only of the different wavelengths used, but also of limb darkening studies at those wavelengths, a technique which proved to be useful in investigating the cloud debris from the Shoemaker-Levy 9 collision with Jupiter (Moreno et al. 1995; Ortiz et al. 1995; Muñoz et al. 1996; Molina et al. 1997). Due to the fact that the coloration of the GRS is sometimes altered by the presence of South Equatorial Belt disturbances, we also report on the possible changes in the GRS particle physical properties before and after the SEBD event that started on 1993 April 6th (see e.g. Rogers, 1993; Sánchez-Lavega et al. 1996; Moreno et al., 1997).

The description of the high-quality observations used here and the reduction technique employed are shown in Sect. 2. The
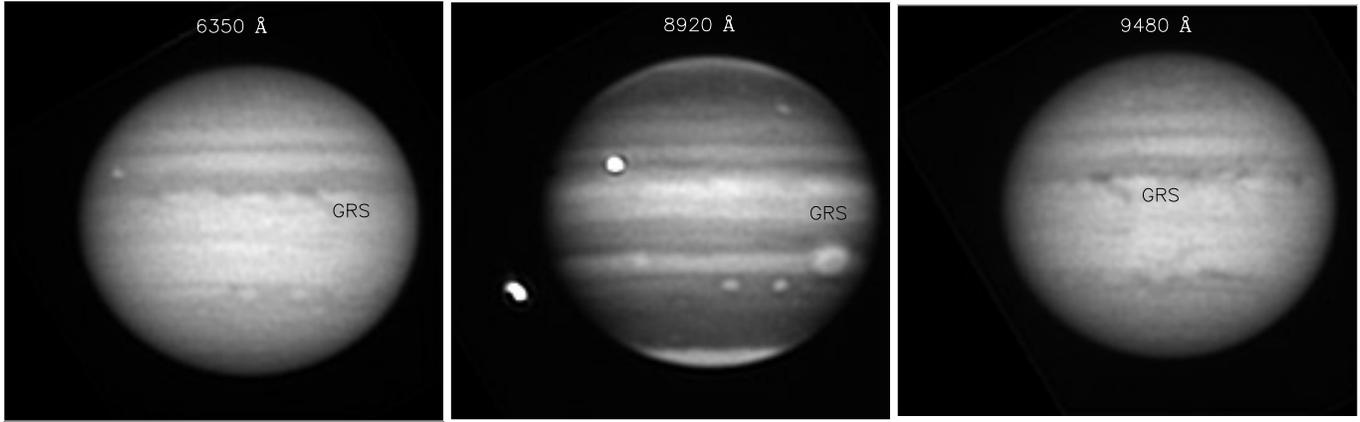

Fig. 1. Sample Jovian images at 6350, 8920 and 9480 Å obtained with the 1.5-m Spanish Telescope at Calar Alto Observatory on 1993 March 11. The GRS is indicated in the figure.

radiative transfer model is described in Sect. 3, and the results are discussed in the last section of the paper.

2. Observations and data reduction

We observed the GRS on Jupiter on four dates: 1993 March 11; 1993 June 4; and 1994 July 18 and 21. The Jovian images were acquired on CCD detectors through narrow-band filters. The observations in 1993 were made at the f/8 focus of the 1.52 m of the Spanish Telescope at Calar Alto Observatory, and the observations of 1994 July were made at the Nasmyth focus of the 4.2 m William Herschel Telescope (WHT) at the Roque de los Muchachos Observatory (La Palma, Spain) during the week of the Shoemaker-Levy 9 impacts on Jupiter. The log of the observations, including the wavelengths of the filters used, is shown in Table 1. All the images were sky subtracted and flat-fielded. During all of these dates, the GRS was tracked from the limb to positions close to the Central Meridian. A sample of the images used in this work showing the range of geometries under which the GRS was observed is shown in Figs. 1–3. The relative reflectivities at the GRS were computed as the average value for a region $2'' \times 2.5''$ in size around the central part of the feature (the longitudinal width of that region was roughly the third part of the longitudinal dimension of the GRS at the time of the observations). The scattering angles (μ, the cosine of Earth's local zenith angle, μ_0, the cosine of the local zenith angle of the Sun, and $\Delta\phi$, the local azimuthal difference between Sun and Earth) of the center of the spot were then computed.

We found a significant difference between the limb darkening coefficient of the GRS (1.08 ± 0.02) and the ambient atmosphere at $-20.5°$ (1.13 ± 0.02) at 8920 Å wavelength. This fact was previously noted by several authors (Clements 1974; West & Tomasko 1980). On the other hand, the limb darkening coefficients at 3600 Å and 9480 Å did not show any differences between the GRS and the ambient atmosphere.

To produce absolute reflectivities, the calibration factors for the images were obtained using the geometric albedoes obtained by Karkoschka 1994. The relative (pixel-to-pixel) error in the derived reflectivities from the images is less than 2%. Adding

Table 1. Jupiter observations on 1993 March 11 and June 4 (1.5 m Spanish Telescope at Calar Alto Observatory), and on 1994 July 18 and 21 (William Herschel Telescope). λ is the wavelength and FWHM is the Full Width at Half Maximum of the filters used in this study

λ (Å)	FWHM (Å)	Scale ("/pixel)	Exposure (s)	Telescope	Date
3600	560	0.102	0.3–1	WHT	Jul '94
3700	150	0.3203	15	CA	Jun '93
4500	150	0.3203	1	CA	Jun '93
5430	100	0.3203	0.5	CA	Jun '93
6350	50	0.3203	1	CA	Mar '93
6450	50	0.3203	2	CA	Jun '93
8920	50	0.3203	8	CA	Mar '93
8920	50	0.3203	2	CA	Jun '93
8920	50	0.102	2–3	WHT	Jul '94
9480	50	0.3203	10	CA	Mar '93
9480	50	0.102	2–3	WHT	Jul '94

this figure to the error in the geometric albedo of 4% claimed by Karkoschka 1994 leads to an upper limit for the absolute I/F values of 6%.

3. The model

In order to retrieve physical properties of the GRS itself, we modelled first the atmosphere in the latitude circle –20.5° planetocentric, but avoiding those points corresponding to the GRS itself. We considered a standard atmospheric distribution comprising three atmospheric layers, a thin haze, an ammonia cloud, and a semi-infinite cloud. This lower cloud was assumed to be composed of particles scattering radiation according to a two-term Henyey-Greenstein phase function given by:

$$P(g_1, g_2, f, \theta) = fP_{HG}(g_1, \theta) + (1 - f)P_{HG}(g_2, \theta)$$

in which P_{HG} is given by:

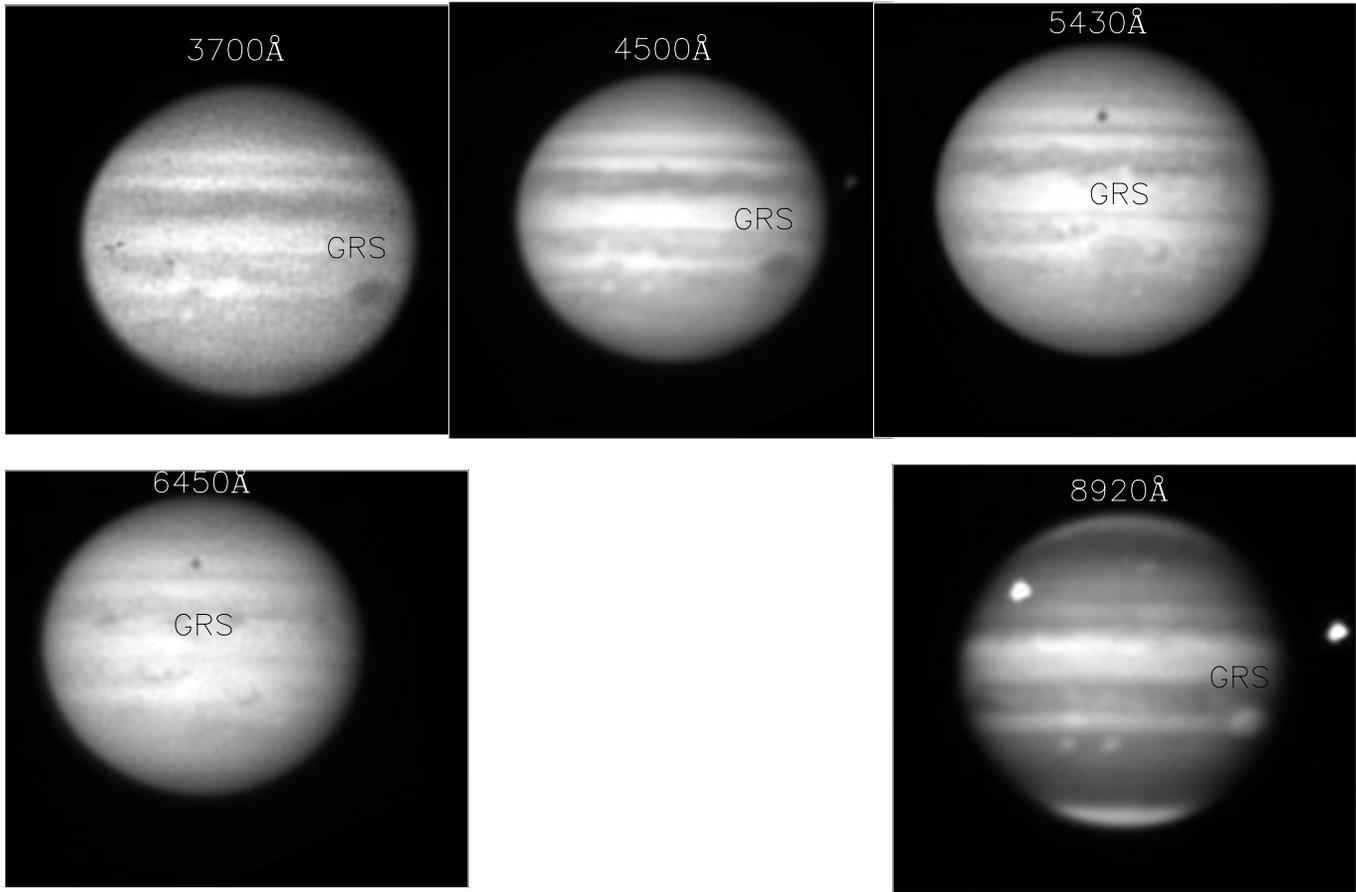$$P_{HG} = \frac{1 - g^2}{(1 + g^2 - 2g\cos\theta)^{3/2}}$$

Fig. 2. Sample Jovian images at 3700, 4500, 5430, 6450 and 8920 Å obtained with the 1.5-m Spanish Telescope at Calar Alto Observatory on 1993 June 4. The GRS is indicated in the figure.
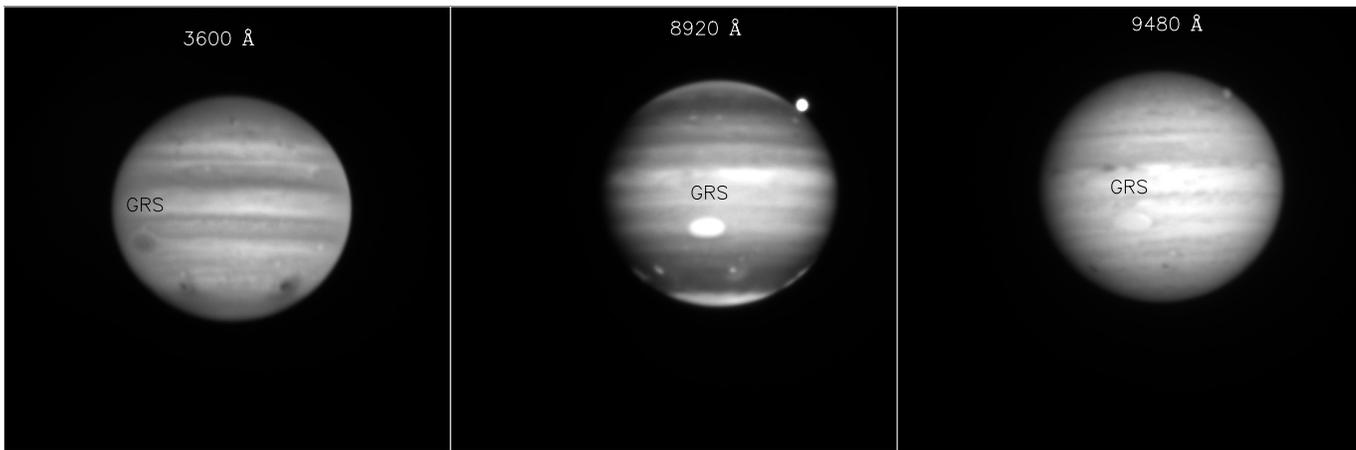

Fig. 3. Sample Jovian images at 3600, 8920 and 9480 Å obtained at the Nasmyth focus of the 4.2-m William Herschel Telescope at La Palma on 1994 July 18. The aerosol debris fields produced after the impacts of fragments of the comet Shoemaker Levy-9 with the planet are clearly seen in the Southern hemisphere.

where θ is the scattering angle and g is the asymmetry parameter. For the present application, we employed g_1=0.8, g_2=-0.8 and f=0.969, i.e., the values given by Tomasko et al. 1978, from Pioneer 10 photometry for the STrZ in the blue region. The single scattering albedo of this semi-infinite cloud was fixed to 0.997, a typical value for the jovian clouds.

The ammonia cloud and the haze layers were assumed to be composed of Mie scattering spheres. In these layers, we set an

Table 2. Atmospheric model at latitude –20.5°S.

pmin (mbar)	pmax (mbar)	N (cm^{-2})	r_m (μm)	n_r (3600 Å)	n_r (9480 Å)	n_i (3600 Å)	n_i (9480 Å)	τ (9480 Å)
100	150	$(4.0\pm0.5)\times10^8$	0.24 ± 0.02	1.6	1.6	0.009 ± 0.002	$(5\pm2)\times10^{-5}$	1.4
400	700	$(4.0\pm0.7)\times10^7$	1.0 ± 0.1	1.47	1.41	6.3×10^{-6}	4.8×10^{-5}	3.5

initial column density of particles distributed with a log-normal size distribution, which is given by:

$$n(r) = N\frac{\exp[-0.5(\ln(r) - \ln(r_m))^2/(\ln(\sigma))^2]}{\sqrt{2}\pi r \ln(\sigma)}$$

where r_m is the modal radius, σ is the width of the distribution, and N is the particle column density. To limitate the number of free parameters, we set σ to 1.2. In each layer, we considered absorption and scattering by particulates and gas. The hydrogen and methane mixing rates were fixed to 0.85 and 1.8×10^{-3} respectively (Gautier et al. 1982). The methane absorption coefficient was calculated by the integration of the Karkoschka 1994 coefficients along the 8920 Å filter transmission curve. We considered as free parameters in the model the size of the particles, the column abundances, the pressure levels in which they are distributed, and their imaginary refractive indices, except for the ammonia cloud, which were taken from Martonchik et al. 1984.

The best fit to the data was obtained following the minimization algorithm by Moreno et al. 1995, by allowing variation in the parameters described above. Once the best fit to the reflectivity data for the latitude circle at –20.5° was obtained, we proceeded to modify this structure in order to model the GRS region. To do that, we introduced particles of different sizes and optical properties (the particles are characterized by a real, n_r, and an imaginary, n_i, refractive indices) from the top of the NH_3 cloud to the top of the model in the stratosphere in order to fit the observational GRS limb darkening curves at the different wavelengths.

4. Results and discussion

The properties of the atmosphere at –20.5° planetocentric were constrained using the highest quality data, which corresponds to the images acquired at the WHT. The best fit to the reflectivity data is shown in Fig. 4 for the different wavelengths at 3600, 8920 and 9480 Å. A haze layer between 100 and 150 mbar, a cloud layer between 400 and 700 mbar, and a semi-infinite cloud at 1750 mbar having the properties given in Table 2 were inferred. In order to find the model structure that better fits the GRS observations, we allowed variations in all the atmospheric structure parameters, except for the physical properties of the ammonia cloud particles and the semi-infinite cloud. The upper and lower levels of the haze layer were varied by allowing a three-layer structure inside that haze layer. Using the procedure by Moreno et al. 1995 again, we found the top and bottom of the GRS haze to be located at different pressure levels than those of the ambient atmosphere, specifically at 2.1 and 450 mbar. We
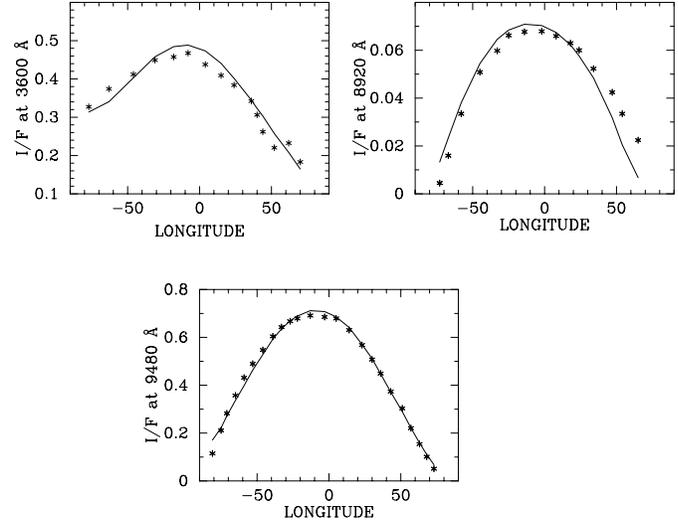

Fig. 4. Resulting model fits for synthetic particle distributions at the three observed wavelengths for the "ambient atmosphere", at the GRS latitude. The asterisks correspond to the observed reflectivity data while the results of the model are represented by solid lines.

Table 3. Vertical distribution of particulates in a region of $2'' \times 2.5''$ centered in the core of the GRS from the analysis of the images obtained on July 1994.

pmin (mbar)	pmax (mbar)	N (cm^{-2})	r_m (μm)	
2.1	85	$(6.5\pm2.0)\times10^7$	(0.18 ± 0.02)	
85	130	$(8.0\pm1.0)\times10^7$	(0.20 ± 0.01)	GRS
130	450	$(8.5\pm1.5)\times10^7$	(0.60 ± 0.05)	particles
450	700	4.0×10^7	1.0	NH_3 Cloud

also inferred different particle sizes for the GRS than for the ambient atmosphere. The differences in refractive indices are, however, not significant. All the relevant inferred parameters for the GRS are shown in Tables 3 and 4. The errors in the column abundances of particles, radii, and refractive indices were estimated by running the best fit model with variations in the input parameters giving absolute reflectivities within the experimental errors shown in Sect. 2. The Minnaert plots comparing the best fit modelled reflectivities with the observed GRS reflectivities are shown in Fig. 5. As shown in Fig. 6, in which the vertical structure found in the GRS and its surroundings is depicted, the atmospheric particulates in the GRS haze extend to higher and lower altitudes than in its neighborhood.

Table 4. Optical properties of the particles.

	Filters	3600 Å	4500 Å	5430 Å	6450 Å	9480 Å
GRS	n_r	1.67	1.67	1.67	1.67	1.67
particles	n_i	$(7.3\pm2.0)\times 10^{-3}$	$(3.0\pm2.0)\times 10^{-3}$	$(7.7\pm2.0)\times 10^{-4}$	$(7.0\pm3.0)\times 10^{-4}$	$(5.0\pm2.0)\times 10^{-5}$
NH$_3$	n_r	1.47	1.446	1.434	1.424	1.410
cloud	n_i	6.3×10^{-6}	2.3×10^{-5}	3.1×10^{-5}	3.8×10^{-5}	4.9×10^{-5}
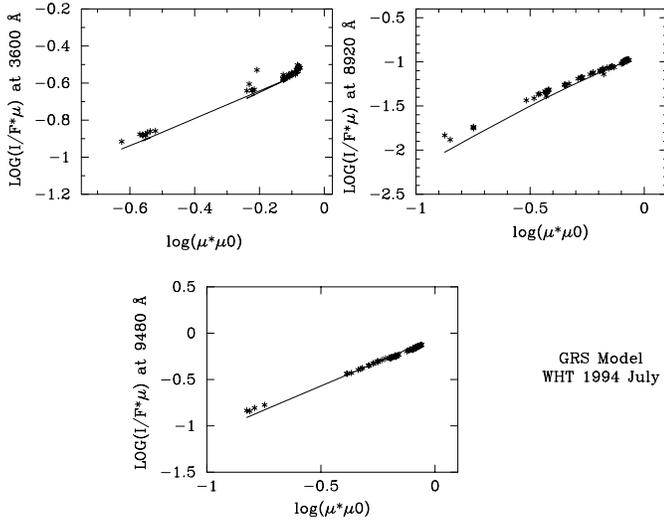
Fig. 5. Minnaert plots of the vertical distribution of particles at the GRS area at the three observed wavelengths on 1994 July at the William Herschel Telescope. The asterisks correspond to the observed reflectivity data while the results of the model are represented by solid lines.

Fig. 6. Graphical representation of the cloud distribution at latitude $-20.5°$ and near the GRS area.

The next step in the modelling procedure was to apply the vertical structure and particle properties of the GRS in 1994 July to the 1993 June dataset. The results were striking: the model matched the GRS 1993 June data, which indicates that the GRS vertical structure did not change between both dates. The results of these model fits for the 1993 June dataset are shown in Fig. 7, for the five wavelengths used.

The GRS particle physical properties found here disagree with the findings of Noy et al. 1981. These authors, from laboratory measurements and a Jovian spectrum from Orton 1975, inferred a value for the particle radius on the GRS of 0.05 μm, while our models indicate the presence of much larger particles. We tried to fit our GRS limb darkening curves by considering a layer of particles, with 0.05 μm in radius and with imaginary refractive indices as given by these authors, placed above the NH$_3$ cloud. Then, by simply varying the top of the ammonia cloud and its single scattering albedo, we could not found any reasonably good fit to the data.

Fig. 8 shows a comparison between the derived imaginary indices for the GRS particles by Noy et al. 1981, and those inferred here. The difference is remarkable, our estimated indices being much lower than those inferred by Noy et al. 1981. The analysis of the Voyager IRIS measurements by Griffith et al. 1992, reveals that the phosphine abundance in the GRS and
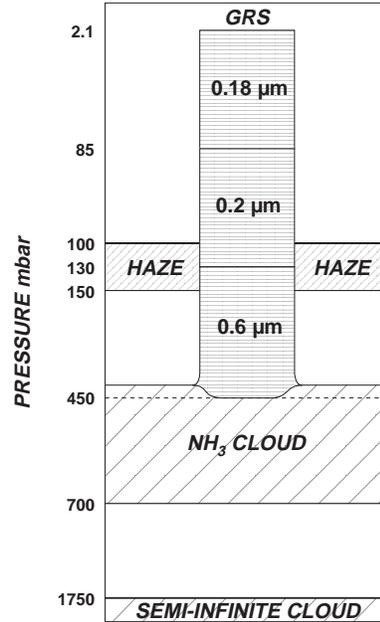
close regions are similar. This fact could indicate that the chemistry of phosphine may not play a special role in the coloration of the GRS, as assumed by Noy et al. 1981, and that the differences between its colour and that of its surroundings is mainly due to a different particle size distribution, as the results of our model indicate.

The next issue to be addressed here is to report on the possible variations in the GRS structure and particle physical properties before and after a SEBD event. As the GRS is located in the boundary of that region, and has been observed to change in colour between the course of these disturbances, it is therefore plausible to find changes in the GRS structure in the course of the event. A comprehensive description of the interaction of the GRS with the spots appearing after a SEBD event is given by Chapman and Reese 1968. As reported by these authors, the GRS is very dark and prominent in the blue and ultraviolet spectral region before the apparition of the disturbance. A few days after the sudden apparition of a dark streak, a lot of dark features are seen which quickly experience eastward motion, and other features also appear but moving toward west longitudes. In a few weeks, some dark spots reach the GRS and then it vanishes, showing very little visual contrast with its neighborhood. A few
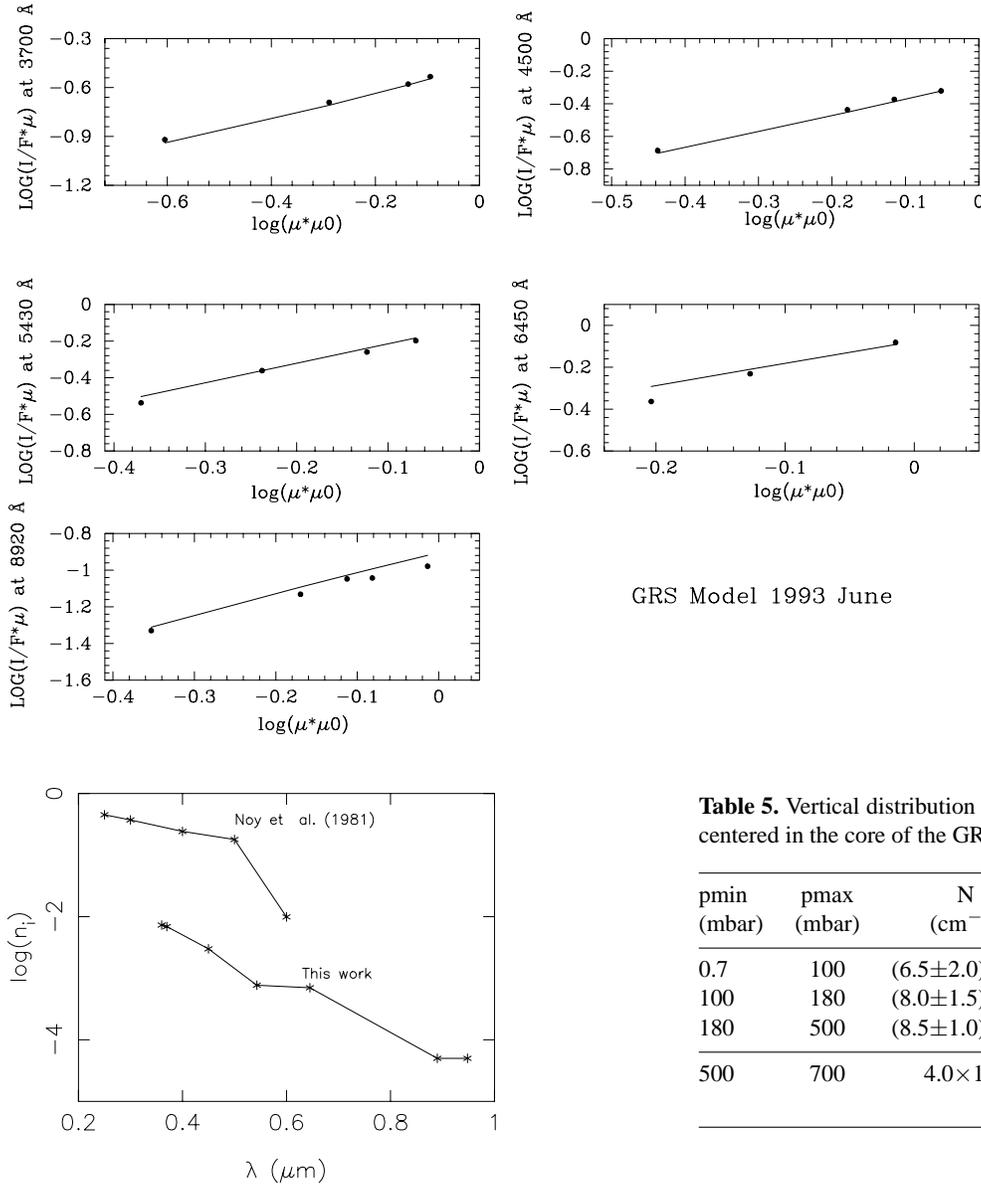
GRS Model 1993 June

Fig. 7. Minnaert plots of the vertical distribution of particles at the GRS area at the five observed wavelengths on 1993 June at the Spanish Telescope of the Calar Alto Observatory. The filled circles correspond to the observed values, while the model is represented by solid lines.

Fig. 8. The variation of the imaginary refractive index of the GRS particles as a function of wavelength and that reported by Noy et al. 1981.

Table 5. Vertical distribution of particulates in a region of $2'' \times 2.5''$ centered in the core of the GRS on 1993 March.

pmin (mbar)	pmax (mbar)	N (cm^{-2})	r_m (μm)	
0.7	100	$(6.5\pm2.0)\times10^7$	(0.18 ± 0.02)	
100	180	$(8.0\pm1.5)\times10^7$	(0.40 ± 0.03)	GRS
180	500	$(8.5\pm1.0)\times10^7$	(0.50 ± 0.05)	particles
500	700	4.0×10^7	1.0	NH$_3$ Cloud

months later, the GRS shows again its normal appearance while the activity of the disturbance ceases.

The last SEBD event was reported to start on 1993 April 6. Our reflectivity measurements made on March 11th, 1993, are therefore well-suited to study the GRS properties before the event and then compare with the GRS structure found in 1993 June and 1994 July, after the SEBD event. The application of the GRS model structure found for the dates after the event to the March 11th 1993 data showed a total disagreement, evidencing the temporal changes in the GRS particle loading and/or physical properties. In order to find the best fit to the data, we kept the values of the refractive indices, assuming there were no changes in this parameter before and after the SEBD event. Under this assumption, the best fit to the March 11th 1993 data

was found for the parameters shown in Table 5, and the corresponding Minnaert plots are shown in Fig. 9. Comparing these results with those obtained after the SEBD event, the following structural differences are found: a) The effective top of the particle layer is placed higher in the GRS atmosphere on 1993 March (0.7 mbar) than on 1993 June (2.1 mbar); b) The particle size is similar from the top to the 100-mbar level on both dates; c) From 100 to 130 mbar there is a particle layer in March 1993 having a larger size (0.4 μm in radius) than the corresponding particles after the SEBD event at those atmospheric levels (0.2 μm in radius). This result indicates that, under the assumption that the particulates over the GRS do not experience changes in their refractive index, the colour changes observed during a SEBD event could be due to changes in particle size.

5. Conclusions

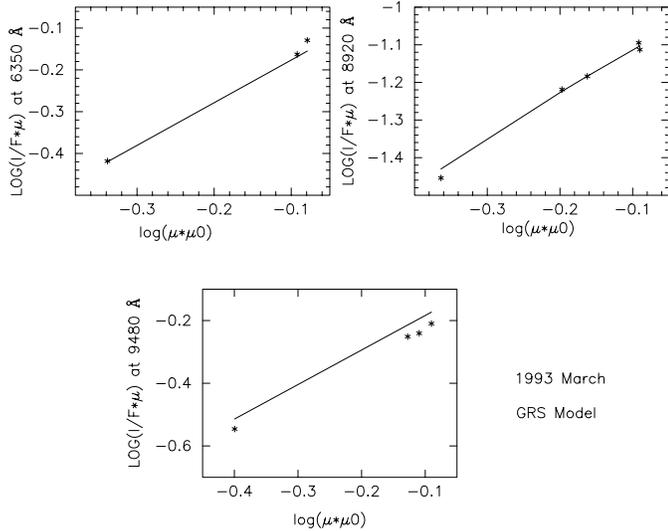The main conclusions of this work can be summarized as follows:

Fig. 9. Minnaert plots of the vertical distribution of particles at the GRS area at the five observed wavelengths on 1993 March at the Spanish Telescope of the Calar Alto Observatory. The asterisks correspond to the observed values, while the best model fit is represented by solid lines.

1. The difference in colour between the GRS on Jupiter and its surroundings could be mainly due to different particle size, rather than to a different composition (different refractive index).
2. We could not detect any change in the GRS structure and particle physical properties just after the SEBD event on June 1993 and a year after that event on July 1994.
3. Under the assumption that the GRS particles are made always of the same material, the GRS structure and particle size changed prior to the 1993 SEBD event with respect to its structure after the SEBD event, having larger radii at levels near 100–130 mbar. A future physical interpretation of this fact should be based on a coupled microphysical-dynamical model.

References

Chapman C.R., Reese E.J., 1968, Icarus 9, 326
Clements A.E., 1974, Ph.D. Dissertation, Univ. of Arizona
Griffith C. A., Bézard B., Owen T., Gautier D., 1992, Icarus 98, 82
Gautier D., Bézard B., Marten A., Baluteau J. P., Scott N., Chedin A., Kunde V., Hanel R., 1982, ApJ 257, 901
Griffith C.A., Bézard B., Owen T., Gautier D., 1992, Icarus 98, 82
Karkoschka E., 1994, Icarus 111, 174
Martonchik J.V., Orton G.S., Appleby J., 1984, Appl. Opt. 23, 541
Molina A., Moreno F., Muñoz O., 1997, Icarus 127, 213
Moreno F., Muñoz O., Molina A., et al., 1995, Geophys. Res. Lett. 22, 1609
Moreno F., Molina A., Ortiz J.L., 1997, A&A 327, 1253
Muñoz O., Moreno F., Molina A., 1996, Icarus 121, 305
Noy N., Podolak M., Bar-Nun A., 1981, J. Geophys. Res. 86, 11985
Ortiz J.L., Muñoz O., Moreno F., et al., 1995, Geophys. Res. Lett. 22, 1605
Orton G.S., 1975, Icarus 26, 159
Peek B.M., 1958, The Planet Jupiter. Faber and Faber, London
Prinn R.G., Lewis J.S., 1975, Sci 190, 274
Ridgway S.T., 1974, BAAS 6, 376
Rogers J., 1993, J. Br. Astron. Assoc. 103, 157
Sánchez-Lavega A., Gómez J.M., Lecacheux J., et al., 1996, Icarus 121, 18
Tomasko M.G., West R.A., Castillo N.D., 1978, Icarus 33, 558
West R.A., Tomasko M.G., 1980, Icarus 41, 278